



Grain refinement, Microstructural characterization, and tensile properties of die-cast AZ91 alloy via Lead and Tin additions

Mohammadreza Askaran, Mehdi Malekan*, Massoud Emamy, Mehrab Lotfpour

School of Metallurgy and Materials Engineering, College of Engineering, University of Tehran, Tehran, Iran.

Received: 9 December 2019; Accepted: 14 December 2019

* Corresponding author email: mmalekan@ut.ac.ir

ABSTRACT

Effects of different amounts of lead (Pb) and tin (Sn) on microstructure and tensile properties of the AZ91 alloy were studied. The results presented that the microstructure of AZ91 alloy is consisted the α -Mg phase and semi-continuous network of β -Mg₁₇Al₁₂ intermetallics. For the as-cast AZ91 alloy, the average grain size and the β phase volume fraction were 96.2 μ m and of 25.3%, respectively. By adding 1 wt.% Pb and 0.5 wt.% Sn, the lowest grain size and volume fraction values obtained. Exceeding Pb and Sn additions have been led to the increasing of the grain size. Furthermore, Sn additions formed the Mg₂Sn intermetallic, while Pb additions didn't form any obvious intermetallics. The Ultimate Tensile Strength (UTS) and tensile elongation (%El) values of the cast AZ91 alloy were 129 MPa and 2.7%, respectively. The optimum amounts of UTS and %El values were achieved by adding 1 wt.% Pb and 0.5 wt.% Sn, respectively. More Pb and Sn additions deteriorated the tensile properties. The fracture surface observations showed that fracture mode in the cast AZ91 alloy was cleavage. Moreover, 1 wt.% Pb and 0.5 wt.% Sn additions altered the fracture mode to more quasi-cleavage fracture.

Keywords: AZ91 cast alloy; Microstructure; Tensile properties; Grain Refinement

1. Introduction

Low density, excellent machinability, high specific strength and stiffness make the magnesium (Mg) alloys profitable for structural applications in the aerospace and automobile industries [1]. Casting Mg alloys have more commercial advantages in comparison with the same wrought alloys because of shorter manufacturing cycles during mass production, leading to lower costs [1,2]. The AZ91 alloy has been supposed to be a favorable alloy due to its desirable casting properties [3]. However, it is essential for industrial applications to solve its deleterious characteristics such as poor corrosion and mechanical properties which can be pertained to the detrimental effects of β -Mg₁₇Al₁₂ phase [3].

Adding alloying elements or grain refiners is an economical route which can readily eliminate the deficiencies and satisfy the industrial demands [1-3]. Recent studies found that additives such as Sc [3], B [4], Bi [5], Sb [5], Sr [6], Ca [7] and rare earth (RE) elements [8] altered the microstructural and mechanical characteristics of the AZ91 alloys. Among various additives, Pb and Sn elements have attracted our attention which numerous studies have investigated their influences on different properties of the AZ91 alloy [9-19].

All of the studies presented that Pb additions could thin the β -Mg₁₇Al₁₂ phase, reduce its volume fraction, make it less continuous and distribute it more homogeneously [9-14]. Furthermore, none

of these studies discerned any trace of Mg_2Pb compound due to its low volume fraction and high solubility of Pb element in Mg [9,12]. Koc et al. [10] illustrated that Pb additions improve the castability of the AZ91 alloy. Hou et al. [12] found that lead has been existed more in the divorced $\beta-Mg_{17}Al_{12}$ intermetallics, then in the interdendritic regions and finally in the lamellar $\beta-Mg_{17}Al_{12}$ intermetallics, respectively. Candan et al. [13] showed that high soluble Pb alloying elements in Mg lower the diffusion of Al and Mg and restrict the formation of the $\beta-Mg_{17}Al_{12}$ intermetallics. Furthermore, 0.4 wt.% Pb addition properly raised the UTS and %El values of the AZ91 alloy due to the inhibiting the formation of $\beta-Mg_{17}Al_{12}$ intermetallics, solid solution strengthening and more homogeneous distribution of refined intermetallics which hindered the crack movements [13]. Bobby et al. [14] also reported the tensile properties enhancements with different Pb additions.

On the other hand, according to previous studies [15-19], low amounts of Sn could diminish the volume fraction of $\beta-Mg_{17}Al_{12}$ intermetallics and change their morphologies from continuous networks of lamellar eutectics to semi-continuous or disconnected divorced eutectics. Furthermore, Turen et al. [15] found that only 0.5 wt.% Sn addition to the AZ91 alloy could increase the fluidity and tensile properties, while adding more than 0.5 wt.% decreased these characteristics. Another study also confirmed the same results in the ZA84 alloy [16]. These studies proved that the presence of Mg_2Sn intermetallics could develop the fluidity and tensile properties, in which high Sn additions coarsened the Mg_2Sn particles and decreased the properties [15,16]. Sedighi et al. [17] showed that 0.5 wt.% Sn addition could refine the microstructure and decrease the grain size through

the formation of Mg_2Sn intermetallics by acting as nucleation sites for the $\alpha-Mg$ phase, while more Sn additions could cluster the Mg_2Sn intermetallics and increase the grain size. Additionally, Mahmudi et al. [18] noted that Sn additions enhanced creep resistance of the AZ91 alloy due to reducing the volume fraction of $\beta-Mg_{17}Al_{12}$ intermetallics, solid solution strengthening effects of Sn element and presence of Mg_2Sn compounds.

Regarding the scarce amounts of studies which investigated the influences of Sn and Pb alloying elements on the relationships between microstructure and tensile properties, in the present study, it has been attempted to achieve a conclusion about changes in correlations between the microstructure and tensile properties of the AZ91 alloy with various Sn and Pb additions.

2. Experimental procedures

In the current study, the AZ91 alloy with 0, 0.5, 1 and 3 wt.% Pb and Sn were fabricated using a high-frequency induction furnace in graphite-ceramic crucible under protective gas atmosphere, containing 95% CO_2 and 5% SF_6 . For producing the AZ91 base alloy, after melting pure magnesium (99.97%) and pure aluminum (99.95%), Al-50 wt.% Zn and Al-18 wt.% Mn master alloys were added to the melt, respectively. Afterward, various amounts of pure Sn (99.93%) and Pb (99.92%), were also combined with the melt at 750 °C (1023 K). Finally, after stirring the melts by a graphite rod and holding them at 1023 K (750 °C) for 5 minutes, all of the casting samples were cast into a cubical iron mold that had been preheated up to 250 °C (523 K). The schematic of samples after casting has been shown in Fig. 1(a). The examined chemical compositions of the alloy specimens have been listed in Table 1.

The existence of intermetallics along the grain

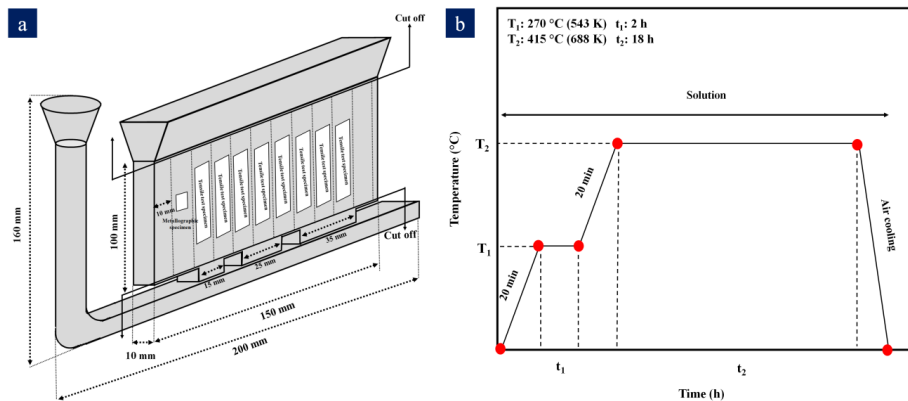


Fig. 1- Schematic drawing of (a) casting specimen, (b) related heat treatment cycles.

boundaries makes it difficult to reveal the grains in the AZ alloys. For this problem, applying heat treatment can dissolve the precipitates into the matrix and unveil the grains. The heat treatment had two cycles in which in the first step, the specimens have been heated at 270 °C (543 K) for 2 hours and then reheated at 415 °C (688 K) for 18 hours followed by air quenching. The schematic of the heat treatment cycles has been shown in Fig. 1(b).

For microstructural analysis, cubic samples with 10 mm × 10 mm × 10 mm dimensions were polished and etched by picral etchant solution (5 ml acetic acid, 5 ml H₂O, 35 ml ethanol, and 1.2 g picric acid) [20]. Microstructural investigations were scrutinized using an optical microscope (OM) and scanning electron microscopy (Vega©Tescan SEM) equipped with an energy dispersive spectrometer (EDS). Linear intercept

method was used to measure the grain size of the specimens according to ASTM E112-13. The X-ray diffraction (XRD) were conducted using Phillips binary x-ray diffractometer with Cu-K α radiation to characterize the phases.

In order to prepare tensile test samples, the casting specimens were machined according to ASTM E8-04 standard. Moreover, the tensile tests were performed using the SANTAM STM-20 digital testing machine with a constant crosshead speed of 1 mm/min at room temperature. The fracture surfaces of the tensile test specimens were also examined with the same SEM equipment.

3. Results and Discussion

3.1 Microstructural Characterization

Fig. 2 presents the OM and related SEM micrographs for the cast and solutionized AZ91 alloy.

Table 1- The examined chemical compositions (wt.%) of the cast specimens

Alloy (wt.%)	Al	Zn	Mn	Sn	Pb	Mg
AZ91	8.97	0.94	0.26	–	–	Bal.
AZ91-0.5%Sn	8.93	0.98	0.29	0.53	–	Bal.
AZ91-1%Sn	8.88	1.03	0.27	0.96	–	Bal.
AZ91-3%Sn	9.03	0.99	0.26	2.98	–	Bal.
AZ91-0.5%Pb	8.96	1.01	0.31	–	0.48	Bal.
AZ91-1%Pb	9.02	0.94	0.32	–	1.09	Bal.
AZ91-3%Pb	8.97	0.96	0.29	–	2.88	Bal.

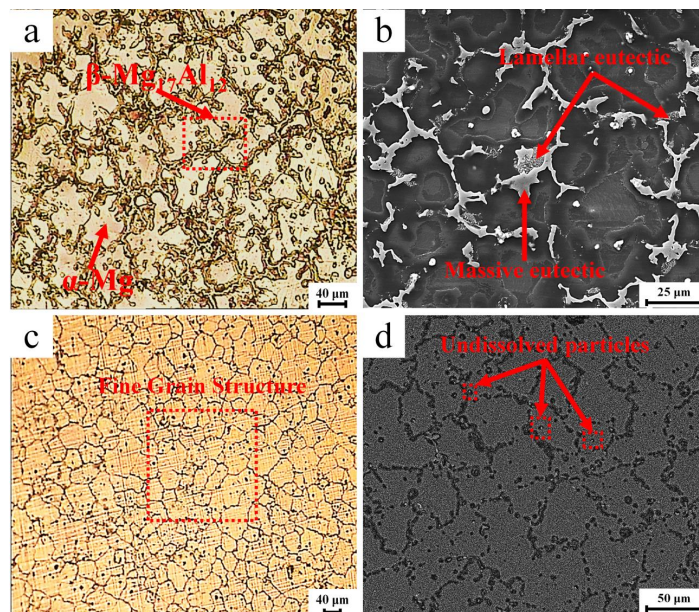


Fig. 2- The optical and SEM micrographs for (a),(b) the as-cast and (c),(d) the solutionized AZ91 alloy.

Fig. 2(a) shows that the AZ91 alloy consists of the α -Mg phase and continuous networks of eutectic which are the β -Mg₁₇Al₁₂ intermetallics according to other studies [9-19]. Furthermore, SEM micrograph of the AZ91 alloy comprises two distinctive bright morphologies of β -Mg₁₇Al₁₂ intermetallics: massive eutectic and lamellar eutectic (see Fig. 2(b)). Additionally, solution treatment dissolves the β -Mg₁₇Al₁₂ intermetallics into the matrix and forms the fine grain structure (see Fig. 2(c) and Fig. 2(d)). Also, some scattered bright particles remain after solution treatment which have been defined as undissolved particles.

Fig. 3 demonstrates the OM and related SEM micrographs of the AZ91 alloy with various amounts addition of Pb and Sn alloying elements.

The microstructure of AZ91-Pb and Sn alloys illustrates cast dendritic features similar to the AZ91 base alloy. However, more investigations with the SEM micrographs show that morphology of the β phase changes from fully divorced eutectics to partially divorced eutectics and vice versa with different Pb and Sn additions. In this case, 0.5 and 1 wt.% Pb additions stimulate the β phase to form more partially divorced eutectics whereas adding 3 wt.% Pb creates more fully divorced eutectics. On the other hand, 0.5 wt.% Sn addition has the highest amounts of partially divorced eutectics, but more than 0.5 wt.% additions reverse the morphology continuously to more fully divorced eutectics. It is noteworthy that the transition in the morphology of the β phase could be related to the

change in the constitutional undercooling ahead of the solid-liquid interface during the early stages of cooling [21,22]. Therefore, Sn and Pb additions can alter the characteristics of the solid-liquid interface and also the related constitutional undercooling. With different Pb additions, no new intermetallics have been observed in the SEM micrographs. On the other hand, in the alloy with high Sn content, there are some new intermetallics, which are shown in Fig. 3(f). Based on other studies [15,16], these particles high probably can be the Mg₂Sn intermetallics. Fig. 4 shows the XRD analysis for the cast AZ91 alloy with 0, 1 and 3 wt.% Pb and Sn additions.

It can be seen that the AZ91, AZ91-1 wt.% Pb and AZ91-3 wt.% Pb alloys contain the α -Mg and β -Mg₁₇Al₁₂ phases. However, the AZ91-1 wt.% Sn and AZ91-3 wt.% Sn alloys show the Mg₂Sn intermetallics in addition to the α -Mg and β -Mg₁₇Al₁₂ phases. According to other studies [9,10] and the Mg-Pb binary phase diagram [23], Pb element has high solid solubility (~ 45 wt.% at 466.2 °C) in the Mg and their main intermetallic is Mg₂Pb, which the existing XRD analysis cannot confirm the formation of Mg₂Pb intermetallics maybe due to their low volume fraction.

For more observations, the SEM micrographs with related point and elemental mapping EDS analysis for the AZ91 alloy with 3 wt. % Pb and Sn additions have been brought in Fig. 5. Pertained EDS point results have been listed in Table 2.

According to the EDS elemental mapping in Fig.

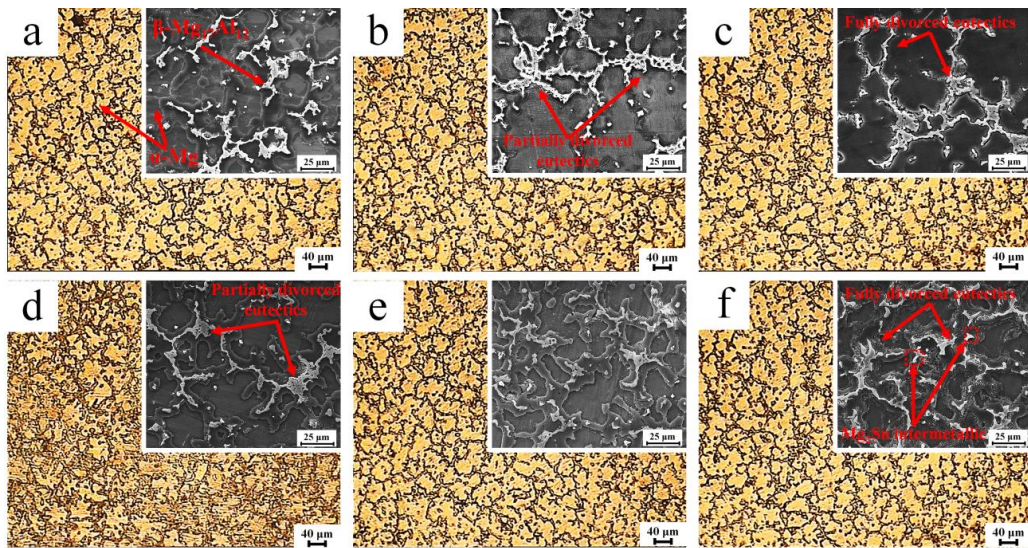


Fig. 3- The optical and related SEM micrographs for the cast AZ91 alloy with (a),(d) 0.5, (b),(e) 1 and (c),(f) 3 wt.% Pb and Sn additions, respectively.

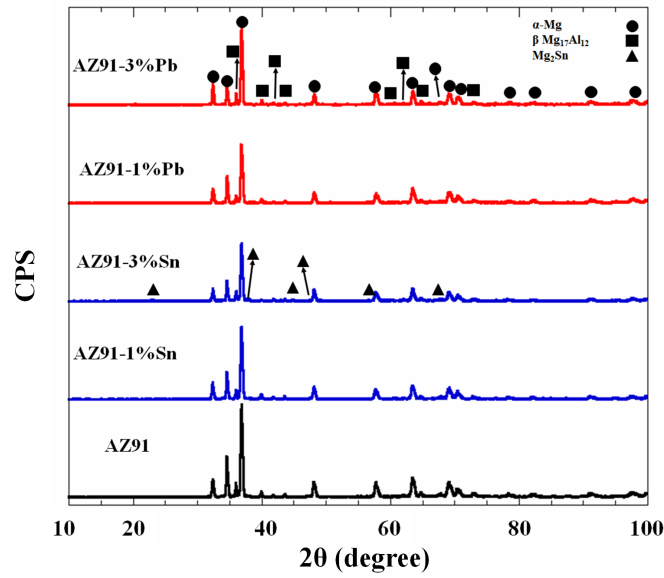


Fig. 4- The XRD patterns of the cast AZ91 alloy with different Pb and Sn contents.

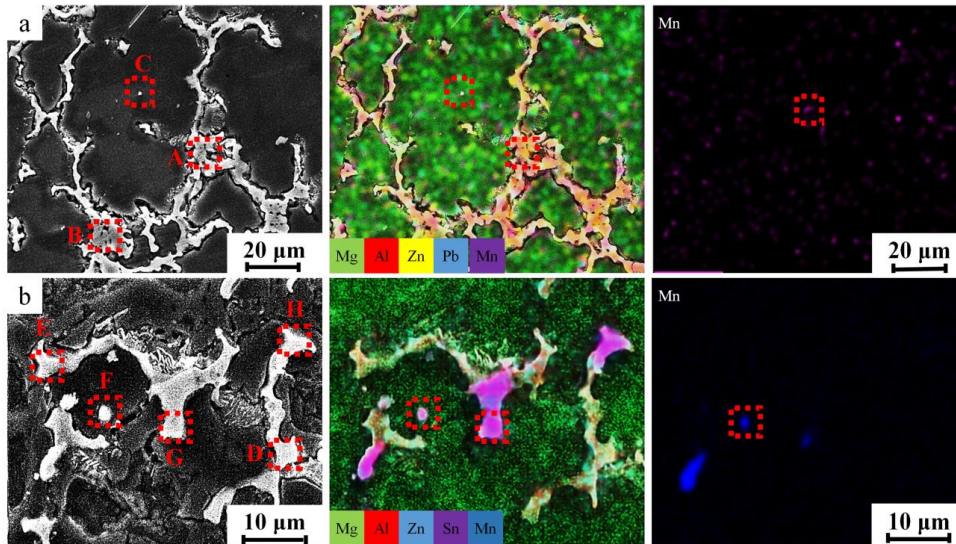


Fig. 5- The SEM micrographs with related point and elemental mapping EDS for the cast (a) AZ91-3%Pb and, (b) AZ91-3%Sn alloys.

Table 2- Results of EDS points in Fig. 5

	Point	Mg (at.%)	Al (at.%)	Zn (at.%)	Mn (at.%)	Pb (at.%)	Sn (at.%)
(a)	A	58.40	36.43	4.52	0.65	0.00	0.00
	B	74.25	24.74	0.27	0.00	0.75	0.00
	C	62.77	34.16	0.00	3.07	0.00	0.00
(b)	D	69.01	29.64	0.92	0.02	0.00	0.41
	E	80.97	17.37	1.08	0.00	0.00	0.59
	F	32.58	42.60	0.31	24.33	0.00	0.17
	G	73.56	3.26	0.02	0.00	0.00	23.16
	H	75.06	2.05	0.21	0.10	0.00	22.58

5(a) and Fig. 5(b), the β -Mg₁₇Al₁₂ intermetallics (marked with A and B) can be found where Al element exists with high concentrations. Also, the Zn element can't be observed in any spots and has been dispersed homogeneously around the microstructure. However, high concentrations of Mn element (marked with C) have been seen in some regions in which its distributions have been brought separately in another figure. Fig. 5(a) demonstrates the homogeneous distribution of Pb element, while Fig. 5(b) illustrates some regions with high concentrations of Sn element (marked with D and E). Based on Table 2, the points (A and B), C and (D and E) in two figures represent the average composition of Mg_{70.66}Al_{27.05}Zn_{1.69}Mn_{0.17}Sn_{0.50}, Mg_{47.67}Al_{38.38}Zn_{0.16}Mn_{13.70}Sn_{0.09} and Mg_{74.31}Al_{2.66}Zn_{0.12}Mn_{0.05}Sn_{22.87} compounds which can be related to the β -Mg₁₇Al₁₂, Al₈Mn₅ and Mg₂Sn intermetallics.

Fig. 6 shows the OM and corresponding SEM micrographs for the AZ91 with diverse Pb and Sn additions after solution heat treatment.

As can be seen, solution treatment not only dissolve the β intermetallics into the matrix but also creates the fine grain structures. However, the SEM micrographs display that solution treatment cannot dissolve some bright intermetallics. According to Fig. 7, the SEM micrographs of solutionized AZ91-1 wt.% Sn and AZ91-3 wt.% Sn alloys and their related elemental mapping EDS

analysis prove the presence of Mg₂Sn and Al₈Mn₅ intermetallics, which can remain after solution treatment due to their high melting points [24]. Also, the undissolved intermetallics in Fig. 2(d) are Al₈Mn₅ intermetallics. The Al₈Mn₅ intermetallics haven't been appeared in the XRD pattern due to their low volume fraction in the alloy.

Fig. 8 represents alterations of the volume fraction of the β intermetallics after casting and the average grain size after solution treatment via different amounts of Pb and Sn alloying elements.

From Fig. 8(a), the volume fraction of β phase in the cast AZ91 alloy is 25.3%, which with adding 3 wt.% Pb and Sn declines to 16.3% and 18.1%, respectively. These reductions occur due to two reasons; (1) the ability of Sn and Pb elements to prevent the diffusion of Al and Mg elements and (2) the formation of larger constitutional undercooling with more Pb and Sn additions, which these two factors inhibit the growth of β -Mg₁₇Al₁₂ intermetallics [11]. In Fig. 8(b), the average grain size value of the solutionized AZ91 alloy is ~96 μ m and adding 1 wt.% Pb reduces the grain size to 41 μ m. However, the grain size value increases a little to 44 μ m with 3 wt.% Pb addition. Moreover, the lowest value of grain size among the Sn-containing AZ91 alloys has been obtained with 0.5 wt.% Sn which is 44 μ m. Further Sn additions increase the grain size value to 47 μ m with 3 wt.% Sn.

Grain refinement role of foreign nucleants or

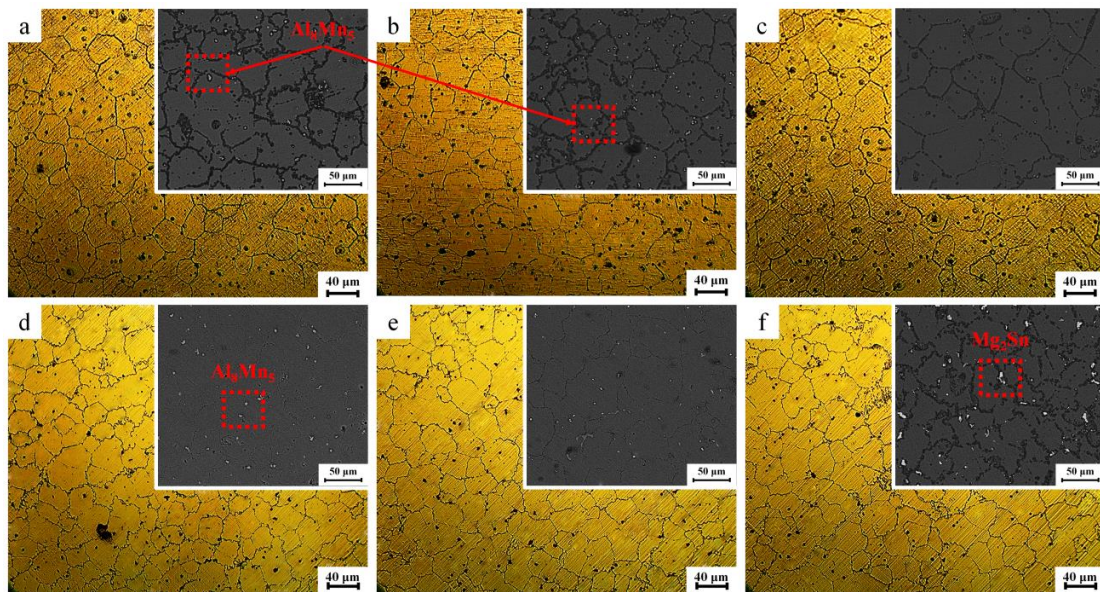


Fig. 6- The optical and related SEM micrographs for the solutionized AZ91 alloy with (a),(d) 0.5, (b),(e) 1 and (c),(f) 3 wt.% Pb and Sn additions, respectively.

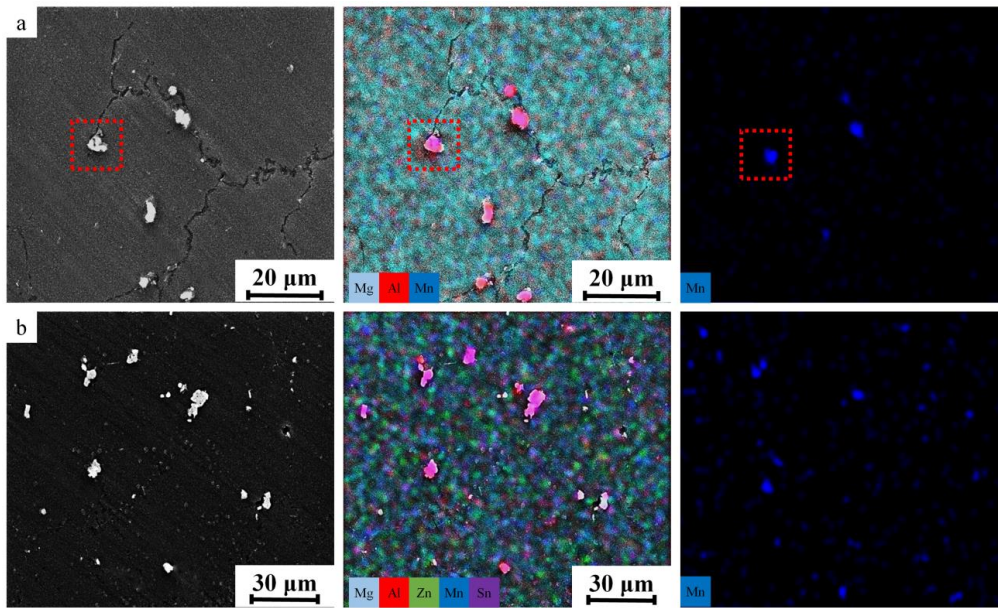


Fig. 7- The SEM micrographs with related elemental mapping EDS for the solutionized (a) AZ91-1%Sn and, (b) AZ91-3%Sn alloys.

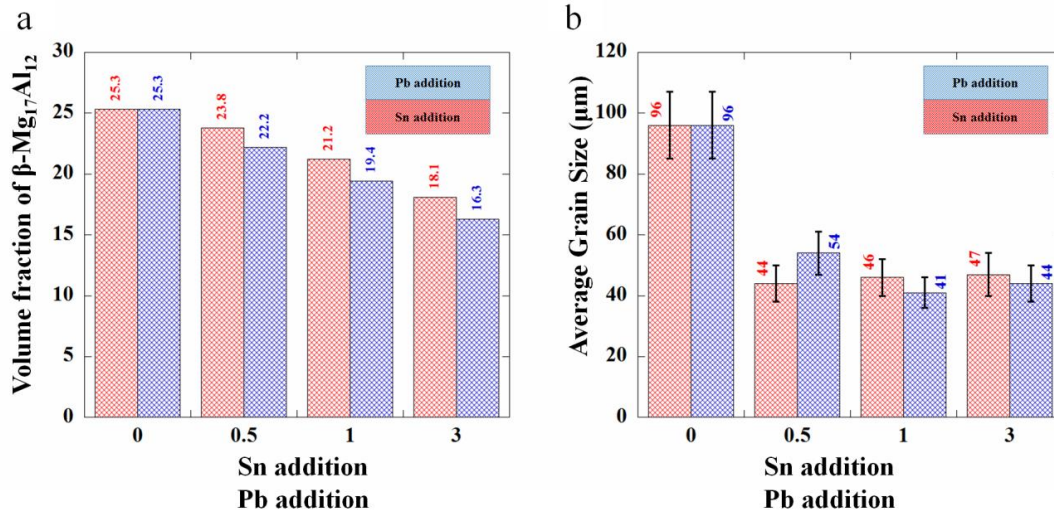


Fig. 8- The variation of (a) volume fraction of $\beta\text{-Mg}_{17}\text{Al}_{12}$ phase in the as-cast alloys and (b) grain size for the solutionized alloys via various Pb and Sn contents.

alloying elements relates to two factors; (1) growth restriction factor (GRF or Q): segregating power of solute and (2) nucleation undercooling: the potency of the nucleant particles [25]. Thus, for distinguishing the grain refinement mechanisms of these two present elements, the Q or GRF values should be calculated. The GRF values obtain from the $Q = \sum_i m_i C_{i,0} (k_i - 1)$ equation, where m_i is the liquidus line slope, k_i is the distribution coefficient

and $C_{i,0}$ is the initial concentration of the element i [25]. The values of $m_i(k_i - 1)$ related to Al, Zn, Mn, Pb and Sn elements have been presented in Table 3. Furthermore, the grain size of the solutionized alloys and related Q values have been listed in Table 4.

As can be seen, GRF values increase with further Pb and Sn additions. Based on other studies [17,26], the Mg_2Sn intermetallics can act as nucleation sites for the $\alpha\text{-Mg}$ phase. Xiang et al. [26] declared that

Mg₂Sn intermetallics could act as the nucleating sites during the solidification process because of their high melting point and low solid solubility in Mg at room temperature. Sedighi et al. [17] studied the thermal analysis of the AZ91 with Sn additions and illustrated that Mg₂Sn intermetallics could have the nucleation potential for the α-Mg phase until 0.5 wt.% Sn addition. By adding more than 0.5 wt.% Sn, the grain size could increase again due to the coarsening of the Mg₂Sn intermetallics [17]. On the other hand, due to high solid solubility of Pb in Mg, the grain refinement can be achieved with the GRF mechanism.

values for the cast AZ91 alloy with different Pb and Sn additions at room temperature.

According to Fig. 9(a), the UTS and %El values of the cast AZ91 alloy are 129 MPa and 2.7%, respectively. Among the Pb-containing alloys, the highest amounts of UTS and %El values have been achieved by 1 wt.% Pb addition, which their related values are 160 MPa and 4.6%, respectively. On the other hand, by adding 0.5 wt.% Sn, the UTS and %El values raises to their optimum stages and their corresponding values are 157 MPa and 3.4%, respectively. However, more Pb and Sn additions (i.e. 3 and 1 wt.%) reduce the UTS and %El values significantly.

3.2. Tensile Properties and Fractography

Fig. 9 presents the alterations of UTS and %El

It is well-known that the initiation and propagation of microcracks have significant effects

Table 3- The values of m, k and m(k-1) related to Al, Zn, Mn, Pb and Sn elements

element	m	k	m(k - 1)	System
Al	-6.87	0.37	4.32	eutectic
Zn	-6.04	0.12	5.31	eutectic
Mn	1.49	1.10	0.15	peritectic
Pb	-2.75	0.62	1.03	eutectic
Sn	-2.41	0.39	1.47	eutectic

Table 4- The values of the grain size of solutionized alloys and related Q amounts

Alloy (wt.%)	Grain size (μm)	Q (K)
AZ91	96	44.5
AZ91-0.5%Pb	54	45.2
AZ91-1% Pb	41	45.9
AZ91-3% Pb	44	48.9
AZ91-0.5%Sn	44	45.0
AZ91-1% Sn	46	45.5
AZ91-3% Sn	47	47.6

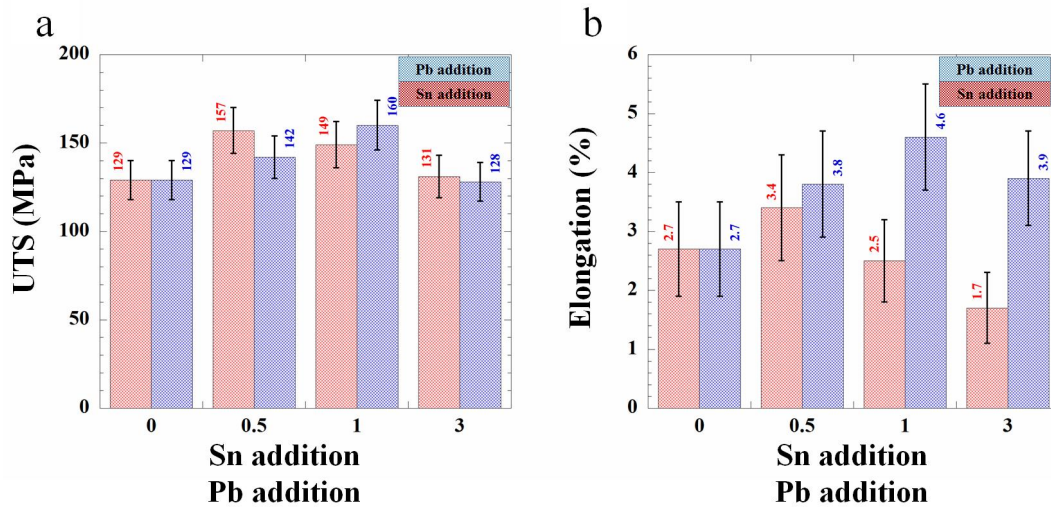


Fig. 9- Variations of (a) UTS and (b) %El values via different Pb and Sn contents for the cast AZ91 alloys.

on the alterations of strength and ductility. In this case, the microcracks can go through their path, join together and form the main cracks. As a result, these main cracks can rupture the surface during the tensile test. In the cast AZ91 alloy, two reasons can generate the microcracks; (1) presence of semi-continuous networks of β -Mg₁₇Al₁₂ intermetallics with high volume fraction and (2) casting defects, which can deteriorate the strength and ductility of the base alloy. Meanwhile, adding Pb and Sn up to 1 and 0.5 wt.% appropriately improve the strength and ductility by four reasons; (1) reducing the volume fraction of β -Mg₁₇Al₁₂ intermetallics and grain size (according to Fig. 8), (2) change the morphology of β -Mg₁₇Al₁₂ intermetallics to the partially divorced shape, (3) solid solution strengthening effects of Pb and Sn elements and (4) presence of Mg₂Sn intermetallics. Turan et al. [15] declared that the transition of lamellar eutectics to fully divorced eutectics could reduce the surface areas that could be led to initiate and propagate the cracks. Thus, in this study, changing morphology to more partially divorced eutectics can decrease the amounts of those areas. Also, It is believed that the Mg₂Sn intermetallics and higher amounts of grain boundaries can significantly delay the crack initiation and propagation and also restrict the dislocations movement by Orowan looping [3,13]. However, more than 1 wt.% Pb and 0.5 wt.% Sn additions, the strength and ductility of alloys

have been deteriorated, due to grain refinement, changing the morphology of β -Mg₁₇Al₁₂ intermetallics to more fully divorced eutectics and coarsening of Mg₂Sn particles [13,15,16]. However, Pb-containing alloys show better tensile properties in higher Pb contents than that for the Sn-containing alloys which can be caused by presence of coarsened Mg₂Sn intermetallics and low solid solution of Sn in Mg matrix [15].

Fig. 10 shows the tensile fracture surfaces (SEM micrographs) for the cast AZ91 alloys with 0, 0.5 wt.% Pb, 1 wt.% Sn and 3 wt.% Pb and Sn additions.

Generally, because of the few activated slip system in hcp crystal structure, fracture mode of Mg alloys at ambient temperature is usually brittle as cleavage or quasi-cleavage form [27]. As can be seen in Fig. 10(a), Fig. 10(c) and Fig. 10(e), the fracture surface of cast AZ91, AZ91-3 wt.% Pb and AZ91-3 wt.% Sn alloys show cleavage failure, because it has a number of cleavage facets (marked with A) and steps (marked with B) and microcracks (marked with C). As declare in the previous paragraphs, microcracks are typically formed from the boundaries between the matrix (i.e. α -Mg phase) and intermetallics (i.e. β -Mg₁₇Al₁₂ and Mg₂Sn compounds) and propagated simply along the grain boundaries. With 0.5 wt.% Sn and 1 wt.% Pb additions, fracture becomes more ductile, which can be caused by the formation of more dimples (marked with D), tearing ridges (marked

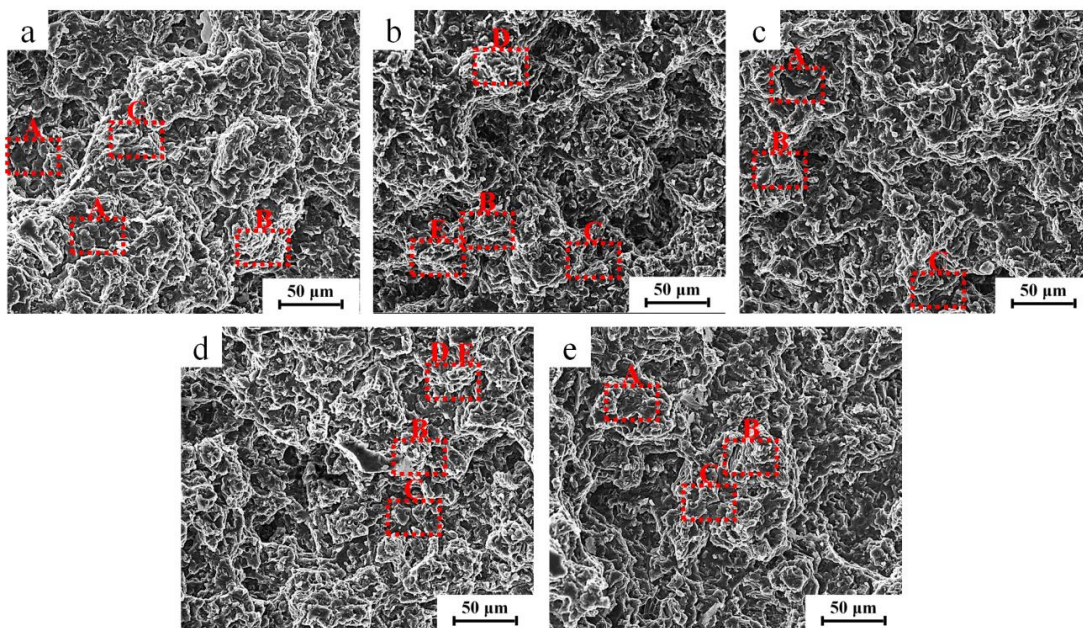


Fig. 10- The SEM micrographs of fracture surfaces for the cast (a) AZ91 (b) AZ91-1 wt.% Pb, (c) AZ91-3 wt.% Pb, (d) AZ91-0.5 wt.% Sn and (e) AZ91-3 wt.% Sn alloys.

with E) and fewer cleavage facets with river patterns (from Fig. 10(b) and Fig. 10(d)). Thus, the fracture mode changes a little to quasi-cleavage rupture with relatively higher elongation values.

4. Conclusions

The effects of different amounts of Pb and Sn elements on the microstructure and tensile properties of the cast AZ91 alloy was investigated. The conclusions have been described below:

(1) The microstructure of cast AZ91 alloy consisted of the α -Mg phase and semi-continuous networks of the β -Mg₁₇Al₁₂ intermetallics. By adding 1 wt.% Pb and 0.5 wt.% Sn, the morphology of the β phase changed from fully divorced eutectics to partially divorced eutectics. The volume fraction of β phase decreased with 3 wt.% Pb and Sn additions. While, no obvious intermetallics were found in the Pb-containing alloys, the Mg₂Sn intermetallics were observed by adding Sn element. After solution heat treatment, the β intermetallics were dissolved and the grain boundaries appeared. The grain size value of the AZ91 alloy decreased with 1 wt.% Pb and 0.5 wt.% Sn additions, respectively.

(2) The UTS and %El values of the AZ91 alloy were 129 MPa and 2.7%, respectively. The optimum UTS and %El values were obtained by adding 1 wt.% Pb and 0.5 wt.% Sn, respectively. More Pb and Sn additions deteriorated the tensile properties by the formation of coarsened Mg₂Sn intermetallics, grain size increment and alteration of partially divorced eutectics to fully divorced one.

(3) The fracture surfaces revealed that the fracture mode of the AZ91 cast alloy was cleavage, which with 1 wt.% Pb and 0.5 wt.% Sn additions, the fracture surfaces showed more quasi-cleavage features.

References

1. Ali Y, Qiu D, Jiang B, Pan F, Zhang M-X. Current research progress in grain refinement of cast magnesium alloys: A review article. *Journal of Alloys and Compounds*. 2015;619:639-51.
2. Pan F, Yang M, Chen X. A Review on Casting Magnesium Alloys: Modification of Commercial Alloys and Development of New Alloys. *Journal of Materials Science & Technology*. 2016;32(12):1211-21.
3. Lin H, Yang M, Tang H, Pan F. Effect of minor Sc on the microstructure and mechanical properties of AZ91 Magnesium Alloy. *Progress in Natural Science: Materials International*. 2018;28(1):66-73.
4. Suresh M, Srinivasan A, Ravi KR, Pillai UTS, Pai BC. Influence of boron addition on the grain refinement and mechanical properties of AZ91 Mg alloy. *Materials Science and Engineering: A*. 2009;525(1-2):207-10.
5. Guangyin Y, Yangshan S, Wenjiang D. Effects of bismuth

- and antimony additions on the microstructure and mechanical properties of AZ91 magnesium alloy. *Materials Science and Engineering: A*. 2001;308(1-2):38-44.
6. Zhang D, Zhang D, Bu F, Li X, Guan K, Yang Q, et al. Effects of minor Sr addition on the microstructure, mechanical properties and creep behavior of high pressure die casting AZ91-0.5RE based alloy. *Materials Science and Engineering: A*. 2017;693:51-9.
7. Wu G, Fan Y, Gao H, Zhai C, Zhu YP. The effect of Ca and rare earth elements on the microstructure, mechanical properties and corrosion behavior of AZ91D. *Materials Science and Engineering: A*. 2005;408(1-2):255-63.
8. Meshinchi Asl K, Masoudi A, Khomamizadeh F. The effect of different rare earth elements content on microstructure, mechanical and wear behavior of Mg-Al-Zn alloy. *Materials Science and Engineering: A*. 2010;527(7-8):2027-35.
9. Çiçek B, Sun Y. A study on the mechanical and corrosion properties of lead added magnesium alloys. *Materials & Design*. 2012;37:369-72.
10. Koc E. Effect of Lead Additions on Microstructure and Casting Properties of AZ91 Magnesium Alloy. *International Journal of Materials Science and Applications*. 2018;7(1):13.
11. Hou H, Zhu T, Wang Y, Gao WEI. EFFECT OF Sn AND Pb ADDITIONS ON MICROSTRUCTURE OF Mg-6Al-1Zn AS-CAST MAGNESIUM ALLOYS. *Modern Physics Letters B*. 2013;27(19):1341023.
12. Hou H, Gao W. Effects of Pb addition on microstructures and elemental distribution of AS-CAST AZ61 Mg alloy. *International Journal of Modern Physics B*. 2017;31(16-19):1744002.
13. Candan S, Unal M, Turkmen M, Koc E, Turen Y, Candan E. Improvement of mechanical and corrosion properties of magnesium alloy by lead addition. *Materials Science and Engineering: A*. 2009;501(1-2):115-8.
14. Boby A, Pillai UTS, Pai BC. Investigation on Lead and Yttrium Addition on the Microstructure and Mechanical Properties of AZ91 Magnesium Alloy. *Journal of Solid Mechanics and Materials Engineering*. 2013;7(2):273-80.
15. Turen Y. Effect of Sn addition on microstructure, mechanical and casting properties of AZ91 alloy. *Materials & Design*. 2013;49:1009-15.
16. Yang M, Pan F. Effects of Sn addition on as-cast microstructure, mechanical properties and casting fluidity of ZA84 magnesium alloy. *Materials & Design*. 2010;31(1):68-75.
17. Sedighi O, Shabestari SG, Yavari F. Investigation on the effect of Sn on solidification and microstructure of AZ91 magnesium alloy using cooling curve thermal analysis. *Thermochimica Acta*. 2018;667:165-72.
18. Mahmudi R, Moeendarbari S. Effects of Sn additions on the microstructure and impression creep behavior of AZ91 magnesium alloy. *Materials Science and Engineering: A*. 2013;566:30-9.
19. Ping W, Jianping L, Yongchun G, Zhong Y, Feng X, Jianli W. Effect of Sn on Microstructure and Electrochemical Properties of Mg Alloy Anode Materials. *Rare Metal Materials and Engineering*. 2012;41(12):2095-9.
20. G. Petzow, V. Carle, *Metallographic etching*, ASM International, 2nd Edition, 2008;114-7.
21. Srinivasan A, Swaminathan J, Gunjan MK, Pillai UTS, Pai BC. Effect of intermetallic phases on the creep behavior of AZ91 magnesium alloy. *Materials Science and Engineering: A*. 2010;527(6):1395-403.
22. Zhao M-C, Liu M, Song G, Atrens A. Influence of the β -phase morphology on the corrosion of the Mg alloy AZ91. *Corrosion Science*. 2008;50(7):1939-53.
23. Nayeb-Hashemi AA, Clark JB. Phase diagrams of binary

magnesium alloys. ASM International, Metals Park, 1988.

24. Ohno M, Mirkovic D, Schmidfetz R. Liquidus and solidus temperatures of Mg-rich Mg–Al–Mn–Zn alloys. *Acta Materialia*. 2006;54(15):3883-91.

25. StJohn DH, Easton MA, Qian M, Taylor JA. Grain Refinement of Magnesium Alloys: A Review of Recent Research, Theoretical Developments, and Their Application. *Metallurgical and Materials Transactions A*. 2012;44(7):2935-49.

26. Xiang Q, Wu RZ, Zhang ML. Influence of Sn on microstructure and mechanical properties of Mg–5Li–3Al–2Zn alloys. *Journal of Alloys and Compounds*. 2009;477(1-2):832-5.

27. Zhang D, Zhang D, Bu F, Li X, Guan K, Yang Q, et al. Effects of minor Sr addition on the microstructure, mechanical properties and creep behavior of high pressure die casting AZ91-0.5RE based alloy. *Materials Science and Engineering: A*. 2017;693:51-9.